Multi-level model predictive control for all-electric ships with hybrid power generation

Haseltalab, Ali; Wani, Faisal; Negenborn, Rudy R.

DOI
10.1016/j.ijepes.2021.107484

Publication date
2022

Document Version
Final published version

Published in
International Journal of Electrical Power and Energy Systems

Electrical Power and Energy Systems 135 (2022) 107484

Contents lists available at ScienceDirect

International Journal of Electrical Power and Energy Systems

journal homepage: www.elsevier.com/locate/ijepes

Multi-level model predictive control for all-electric ships with hybrid power generation

Ali Haseltalab *, Faisal Wani, Rudy R. Negenborn

Department of Maritime and Transport Technology, Delft University of Technology, Delft, the Netherlands

ARTICLE INFO

Keywords:
DC power and propulsion system
Voltage stability
Model predictive control
Hybrid power generation
All-electric ships

ABSTRACT

Power availability to preserve propulsion is a vital issue in the shipping industry which relies on persistent power generation and maintaining the stability of the power and propulsion system. Since the introduction of on-board all-electric Direct Current Power and Propulsion Systems (DC-PPS) with hybrid power generation, which are more efficient compared to direct-diesel and Alternating Current (AC) all-electric configurations, there have been extensive investigations on stabilization and power generation control to enable robust and reliable performance of DC-PPS during different ship operations. In this paper, a multi-level approach is proposed for hybrid power generation control. For this goal, first, a mathematical model is proposed for each power system component and then, the overall on-board power system is modeled in a state space format. Then, a multi-level Model Predictive Control (MPC) approach is proposed for the DC voltage control which unlike conventional droop control approaches, takes the DC current generated by power sources into account explicitly. The performance of the proposed approach is evaluated via several simulation experiments with a high fidelity model of a high voltage DC-PPS. The results of this paper lead to enabling more effective approaches for power generation and stability control of constant power loaded microgrids.

1. Introduction

Due to the regulations imposed by international maritime authorities, the shipping industry is working extensively towards reducing its environmental impact. The reduction of emissions and increasing the fuel efficiency are being pursued by applying different design and energy management strategies. Over the last few decades, in order to enable the optimal use of the energy sources, one of the main strategies has been the introduction of novel and more fuel efficient power and propulsion system configurations. These advanced power and propulsion systems are regarded as substitutions for the conventional direct-diesel configuration in which the relationship between the propeller and the diesel engine is established directly through a drive shaft. The transformation to advanced power and propulsion systems leads to a more efficient energy conversion and a more effective fuel conservation. One of these new configurations is *all-electric* Direct Current Power and Propulsion System (DC-PPS) configuration where the relationship between the power sources and propellers is established through a DC microgrid [1,2]. In principle, the notion of all-electric is used for ships in which the relationship between power sources and loads is established through an electrical network [2,3].

With the advances in the domain of semiconductors, DC-PPS is known as one of the most fuel-efficient configurations [1]. In this configuration, the mechanical power generated by the diesel engine(s) is converted into electrical power by synchronous generator(s). The Alternating Current (AC) voltage and current of the generators are then converted to DC using rectifiers which are connected to the DC grid (DC-link). The battery is also connected to the same grid through a bidirectional converter. The propellers are connected to the DC grid through sets of motor controller inverter-induction machines. A schematic view of a DC-PPS is shown in Fig. 1.

Propulsive power availability is dependent on the robustness and stability of the DC-PPS. The on-board energy sources should be able to generate power in parallel and prevent blackouts by means of cooperative control.

One of the main barriers in enabling DC-PPS for widespread use is the problem of DC grid voltage stability and control of Diesel-Generator-Rectifier (DGR) sets as well as battery-converter sets [4,5]. Alongside with the lack of feasible fault-detection and isolation strategies, the absence of viable power generation control strategies is considered as

* Corresponding author.
E-mail addresses: a.haseltalab@tudelft.nl (A. Haseltalab), f.m.wani@tudelft.nl (F. Wani), r.r.negenborn@tudelft.nl (R.R. Negenborn).

https://doi.org/10.1016/j.ijepes.2021.107484
Received 17 July 2020; Received in revised form 22 July 2021; Accepted 4 August 2021
Available online 13 August 2021

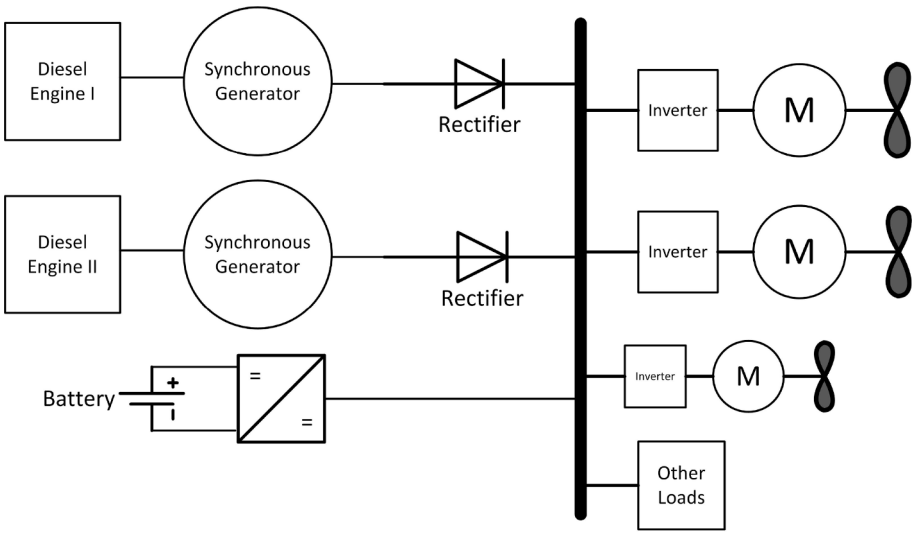

Fig. 1. The DC-PPS under study.

one of the main challenges in enabling DC-PPS [2]. The problem of stability is even more complex if uncontrollable passive six-pulse rectifiers are used for AC/DC conversion [6]. Highly nonlinear dynamics of DGR and battery-converter sets as well as adverse effects of Constant Power Loads (CPL) are among the reasons that negatively affect the power generation quality and cause instability [4,6].

1.1. Literature review

The stability issue of DC microgrids has received extensive investigation in academia and industry over the last few years. The solutions to address this issue range from configuration and architectural solutions to systems and control solutions. In the literature, several architectural solutions have been proposed to improve the power quality [7] of DC microgrids including addition of energy storage modules [8], load shedding [9], the adoption of virtual impedance [10], and filtering methods for reducing oscillation [11,12].

The stabilization of DC microgrids in the presence of CPLs has been studied in several research works. In [13], the stability of DC microgrids with uncertain CPLs is studied where it is assumed that the CPL's power is varying. The stability analysis of DC microgrids in the presence of multiple DC-DC converters loaded with CPLs is carried out in [14] and then, two linear control approaches are proposed to stabilize the grid. Semidefinite programming approaches are used for stability analysis and control of DC microgrids in [15]. In [16], a disturbance observer feedforward compensation scheme is proposed for voltage control using a cascaded power converter.

In most of the DC microgrids, there are multiple power generators, such as diesel-generators, batteries, and fuel cells, which are connected to the grid through power converters. The diverse dynamics of these power generators make the grid to be a multi-time scale system. The dynamic modeling of multi-time scale DC microgrids is investigated in [17] and their low frequency stability is analyzed in [18]. Decentralized, distributed, and hierarchical control approaches are used to stabilize DC microgrids in [19,20]. In [19], a distributed control approach is proposed to achieve voltage stability by controling the state of charge of DC electric springs. In [20], the DC voltage of the grid is controlled using a hierarchical control scheme in the presence of renewable energy sources and energy storage modules. A decentralized control approach is proposed in [21] to guarantee stability through controlling the generated DC current of power sources. A review on control of DC microgrids is given in [22].

Over the last few years, advanced and novel control strategies have been adopted for DC-PPS. In [23], a distributed adaptive control approach is applied to a zonal ship power system and then, the interaction between on-board AC and DC networks is studied. The adoption and control of multi-level isolated DC-DC converters is discussed in [24]. In [25], a feedback linearizing control approach is proposed for voltage regulation and speed control of diesel-generators. A Model Predictive Control (MPC) approach is used for control of a diesel-generator-rectifier set and voltage stabilization in a DC-PPS in [6].

In all of the research papers mentioned, the focus is on active rectification, i.e., there is a controller at the AC/DC converting stage for the voltage control. However, compared to passive uncontrolled rectifiers, active rectifiers are more expensive, require more maintenance, and take more space in the switchboard. As a result, the passive six-pulse rectifiers are considered more favorable by the maritime industry. Moreover, in the literature, the study of DC-PPS stability is limited compared to energy management and efficiency studies [1,26], while one of the main drawbacks of enabling DC-PPS with hybrid energy sources is the lack of appropriate control approaches. Such control schemes coordinate the controllers of different on-board energy sources, i.e., DGR sets and battery-converter sets, to achieve reliable and robust ship performance [2].

1.2. Contributions of this paper

Considering the insufficiency of linear droop control approaches to address the stability concerns [27], in this paper, a multi-level MPC approach is proposed for the control of DC voltage of the grid which is the main DC-PPS stability indicator as well as shaft speed control of diesel-generators. To design the control approach, first a dynamical model for every component in the power system is presented and then, by combining the models a state space model for the on-board DC power system is created. For power generation control that is DC-link voltage control and control of diesel-generators shaft speed, by using the results in [6], a multi-level MPC control approach is proposed. On the top level a coordinating controller is considered which determines the required DC current to keep the DC voltage around its nominal value. Through this controller, the reference DC currents are calculated, which are sent to the controllers on the second level. These so-called low level controllers aim at controlling the generated current by the energy sources.

In a DC-PPS, the DC-link voltage fluctuates as a result of voltage conversion and rectification. Moreover, due to the existance of different load types, uncertainty and disturbances might appear in the form of DC current. As a result, in the proposed control approach, the coordinator uses a tube-based MPC approach [28], that is a robust control scheme, for DC voltage control and determination of the reference DC current.

The low level controllers use an MPC approach to follow the reference current. Input-Output Feedback Linearization (IOFL) is used to linearize the model. Moreover, a constraint linearization technique [29,30] is adopted to enable the use of quadratic programming approaches for solving the optimization problem of the MPC-based controllers. As a result, the controllers are capable of operating with short sampling times. The performance of the proposed approach is evaluated using a high voltage DC-PPS model with high fidelity component models which are provided by our industrial project partner. Voltage control under varying loads and short circuit faults are considered for simulation experiments. The main contributions from this paper can be summarized as:

1. Control for DC-PPS with hybrid power generation using six-pulse passive rectifiers in the presence of CPLs which has not so far been considered in the literature.
2. Deriving a state space model for the on-board DC power system which is suitable for stability studies and power generation controller design.
3. Proposing a multi-level MPC approach that guarantees the stability of the DC-PPS by controlling the DC-link voltage and the shaft speed of the diesel-generators. IOFL as well as a method for constraint linearization are adopted to enable the use of quadratic programming for solving the optimization problem of the MPC controllers.

1.3. Outline

The remainder of this paper is organized as follows. In Section 2, a model for every component in a DC on-board power system is presented and then, a state space model is derived for the energy generation side. The proposed control strategy is proposed in Section 3 and the relationship with the energy management module and autopilot control module is explained. In Section 4, the performance of the proposed control approach is evaluated through several simulation experiments on a high voltage DC-PPS. Conclusions and future research directions are given in Section 5.

2. DC-PPS state space modeling

In this section, after describing a DC-PPS, a dynamical model for every component is proposed and then, a the overall state space model of the energy generation side in a DC-PPS is derived.

In a DC-PPS the mechanical power generated by diesel engines is transferred in form of electrical power, after which it is converted into mechanical power by electric motors for propulsion. A DC-PPS has several prime movers that are normally diesel-generators which are connected to the DC-link through rectifiers which convert AC voltages and currents to DC. One of the advantages of DC-PPS is simple integration of new energy sources such as batteries [26], ultracapacitors [31], and fuel cells [32]. Therefore, normally a battery is also connected to the DC-link through a bidirectional converter that enables charge and discharge modes. On the energy consumption side of a DC-PPS, induction motor-propeller sets are connected to the DC-link by motor controller inverters. Other on-board loads are also connected to the DC-link. Among several advantages of DC-PPS optimal engine loading, variable diesel engine speed, increased fuel efficiency, decreased number of converting stages, and more flexibility in design can be realized [26,33]. However, the lack of feasible power generation control and fault-detection and isolation strategies are main bottlenecks in enabling DC-PPS [2].

In this section, a state space model for the on-board DC power system is proposed which is later used for the design of a multi-level model predictive power generation control approach. The power system components in a DC-PPS are diesel engines(s), synchronous generator(s), rectifier(s), battery, bidirectional converter, and the DC-link. In this paper, to replicate realistic DC-PPS loading condition during the ship operation, it is assumed that the power system is loaded with a CPL with a varying power over time.

2.1. Diesel engine

The diesel engine dynamics can be approximated by nonlinear or linear equations (see, e.g., [34,35]), depending on the level of accuracy needed. To establish the relationship between the fuel index and produced torque Q_{en}, a linear model [36] is used, that is:

$$\dot{Q}_{en}(t) = -\frac{1}{\tau_{en}}(Q_{en}(t) + K_{en} f_{en}(t)), \tag{1}$$

where K_{en} is the torque constant, f_{en} is the governor setting (i.e., fuel index and flow) and τ_{en} is the torque buildup constant which determines the response speed of the diesel engine, a function of diesel-generator shaft speed:

$$\tau_{en} = \frac{0.9}{\omega_{dg}}, \tag{2}$$

where ω_{dg} represents the rotational speed in rad/s [37].

2.2. Synchronous generator

The relationship between a generator and a diesel engine is established through the shaft speed where the generated torque of the diesel engine is an input for the generator. In this paper, the Park equivalent Direct-Quadratic (dq) modeling approach is used to represent the dynamics of the synchronous generator [38]. The relationship between the voltages, fluxes, and currents in the dq reference frame is established using the following equations:

$$\begin{aligned}
\dot{\psi}_d(t) &= -v_d(t) + \omega_{dg}(t)\psi_q(t) + r_s i_d(t) \\
\dot{\psi}_q(t) &= -v_q(t) + \omega_{dg}(t)\psi_d(t) + r_s i_q(t) \\
\dot{\psi}_{fd}(t) &= v_{fd}(t) - r_{fd} i_{fd}(t) \\
\dot{\psi}_{kd}(t) &= -r_{kd} i_{kd}(t) \\
\dot{\psi}_{kq}(t) &= -r_{kq} i_{kq}(t),
\end{aligned} \tag{3}$$

where r_s, r_{fd}, r_{kd}, and r_{kq} are stator, field circuit and damping resistances, respectively. Variables ψ_d and ψ_q are fluxes in the d and q axis, ψ_{kd} and ψ_{kq} are damper fluxes; field flux is represented by ψ_{fd}. In the above model, v_d and v_q are dq voltages and v_{fd} is the field voltage of the generator. The mechanical dynamics of the synchronous generator are given as:

$$\dot{\omega}_{dg}(t) = \frac{1}{2H}\left(\psi_d(t) i_q(t) - \psi_q(t) i_d(t) + Q_{en}(t)\right), \tag{4}$$

where ω_{dg} is the shaft speed of the diesel generator, Q_{en} is the mechanical torque produced by the diesel engine, and $H = \frac{J}{p}$ is the inertia constant per pole. Using the system inductances, the relationship between electrical currents and fluxes can be established as:

$$\begin{bmatrix} i_d(t) \\ i_q(t) \\ i_{fd}(t) \\ i_{kd}(t) \\ i_{kq}(t) \end{bmatrix} = \begin{bmatrix} -L_d & 0 & L_{md} & L_{md} & 0 \\ 0 & -L_q & 0 & 0 & L_{mq} \\ -L_{md} & 0 & L_{fd} & L_{md} & 0 \\ -L_{md} & 0 & L_{md} & L_{kd} & 0 \\ 0 & -L_{mq} & 0 & 0 & L_{kq} \end{bmatrix}^{-1} \begin{bmatrix} \psi_d(t) \\ \psi_q(t) \\ \psi_{fd}(t) \\ \psi_{kd}(t) \\ \psi_{kq}(t) \end{bmatrix}, \tag{5}$$

where $L_d, L_{md}, L_{kd}, L_{fd}, L_q, L_{mq}$ and L_{kq} are per unit inductances [39].

2.3. Rectifier and the DC-link

We consider an average value model with constant parameters for the uncontrollable rectifier [40]. In our model, the rectifier is introduced with generator currents as input and DC current as the output. The DC current can be computed as:

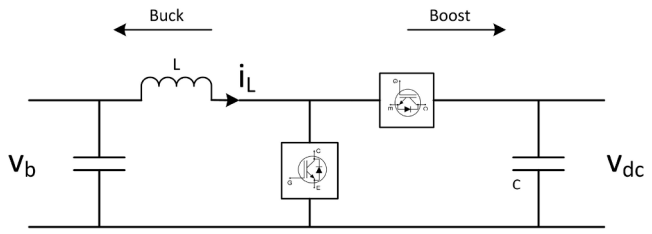

Fig. 2. The circuit diagram of the bidirectional converter.

$$i_{dc}(t) = \beta_{rec}\sqrt{i_q^2(t) + i_d^2(t)} \tag{6}$$

where β_{rec} is an efficiency constant. The DC-link voltage is derived using the Kirchhoff's equation as:

$$\dot{v}_{dc}(t) = \frac{1}{C}(i_{dc}(t) - i_{load}(t)), \tag{7}$$

where i_{load} is the DC load current that is $i_{load} = \frac{P}{v_{dc}}$ with P denoting the CPL power.

The dq-voltages from the rectifier to the generator are as follows:

$$\begin{aligned} v_q(t) &= \alpha_{rec} v_{dc}(t)\cos(\theta_g) \\ v_d(t) &= \alpha_{rec} v_{dc}(t)\sin(\theta_g), \end{aligned} \tag{8}$$

where θ_g is the load angle, computed as:

$$\theta_g = \arctan\left(\frac{i_d(t)}{i_q(t)}\right) - \phi_{rec}. \tag{9}$$

Variables $\alpha_{rec}, \beta_{rec}$ and ϕ_{rec} are considered constant in this model.

2.4. Battery

A model from [41] is used for representing the battery dynamics. This model is suitable for power and energy management purposes. The State-of-Charge (SoC) of the battery is determined using:

$$S_{oC}(k+1) = S_{oC}(k) - \left(\frac{\eta_i \Delta t}{C_n}\right) i_b, \tag{10}$$

where η_i is the cell Coulombic efficiency, i.e., $\eta_i = 1$ for discharge and $\eta_i \leqslant 1$ for charge. Parameter C_n is the nominal capacity of the battery, k is the sampling time, Δt is the sampling period, and i_b is the battery current. The battery voltage can be derived as:

$$v_b = O_{CV}(S_{oC}(k)) - r_b i_b, \tag{11}$$

where O_{CV} is the open circuit voltage of the battery, being a function of S_{oC}, and r_b is the battery resistance.

2.5. Bidirectional converter

A non-isolated bidirectional converter is considered for the DC-PPS. Non-isolated bidirectional converters are suitable for low and medium voltage DC microgrids. They are cheaper and have lower losses compared to isolated converters. The structure of the converter is shown in Fig. 2.

The dynamical model of the converter is adopted using Kirchhoff's current and voltage laws:

$$\begin{aligned} \dot{i}_L &= \frac{d(t)}{L} v_{dc}(t) - \frac{v_b(t)}{L} \\ \dot{v}_{dc} &= \frac{D}{C} i_L(t) - \frac{i_{load}(t)}{C}, \end{aligned} \tag{12}$$

where $d(t)$ is the duty cycle of the switching operation, i_L is the current of the equivalent inductor on the low voltage side of the converter, v_b is the battery voltage and D is the voltage ratio. The converter is controlled using a cascaded PID control approach [42].

2.6. State space modeling of energy generation side

In this part, a state space model is presented that combines the components of the energy generation side. For the sake of simplicity in presenting the equations, the time indication t is dropped. First, (3) is rewritten in matrix form as:

$$\begin{bmatrix} \dot{\psi}_d \\ \dot{\psi}_q \\ \dot{\psi}_{fd} \\ \dot{\psi}_{kd} \\ \dot{\psi}_{kq} \end{bmatrix} = \begin{bmatrix} 0 & \omega_{dg} & 0 & 0 & 0 \\ \omega_{dg} & 0 & 0 & 0 & 0 \\ 0 & 0 & 0 & 0 & 0 \\ 0 & 0 & 0 & 0 & 0 \\ 0 & 0 & 0 & 0 & 0 \end{bmatrix} \begin{bmatrix} \psi_d \\ \psi_q \\ \psi_{fd} \\ \psi_{kd} \\ \psi_{kq} \end{bmatrix} + \begin{bmatrix} r_s & 0 & 0 & 0 & 0 \\ 0 & r_s & 0 & 0 & 0 \\ 0 & 0 & -r_{fd} & 0 & 0 \\ 0 & 0 & 0 & -r_{kd} & 0 \\ 0 & 0 & 0 & 0 & -r_{kq} \end{bmatrix} \begin{bmatrix} i_d \\ i_q \\ i_{fd} \\ i_{kd} \\ i_{kq} \end{bmatrix} + \begin{bmatrix} v_d \\ v_q \\ v_{fd} \\ 0 \\ 0 \end{bmatrix}. \tag{13}$$

Then, by combining (13) with (5) and (8), we obtain:

$$\dot{I}_G = X_G^{-1} S_\omega(\omega_{dg}) X_G I_G + X_G^{-1} R_G I_G + v_{dc} X_G^{-1} \begin{bmatrix} \alpha_{rec}\sin(\arctan(\frac{i_d}{i_q}) - \phi_{rec}) \\ \alpha_{rec}\cos(\arctan(\frac{i_d}{i_q}) - \phi_{rec}) \\ 0 \\ 0 \\ 0 \end{bmatrix} + X_G^{-1} b v_{fd}, \tag{14}$$

where $I_G = [i_d, i_q, i_{fd}, i_{kd}, i_{kq}]^T$ is the vector of currents, X_G is the matrix of per unit inductances defined in (5), and R_G is the diagonal matrix of resistances shown in (13). Moreover,

$$S_\omega(\omega_{dg}) = \begin{bmatrix} 0 & \omega_{dg} & 0 & 0 & 0 \\ \omega_{dg} & 0 & 0 & 0 & 0 \\ 0 & 0 & 0 & 0 & 0 \\ 0 & 0 & 0 & 0 & 0 \\ 0 & 0 & 0 & 0 & 0 \end{bmatrix}$$

and $b = [0 \quad 0 \quad 1 \quad 0 \quad 0]^T$.

The dynamics of a diesel-generator shaft speed can now be represented in matrix form as:

$$\begin{aligned} \dot{\omega}_{dg} &= \frac{1}{2H}(Q_{en} - I_G X_G^T G_1 I_G) \\ \dot{Q}_{en} &= -\frac{Q_{en}}{\tau_s} + K_{en} f_{en}, \end{aligned} \tag{15}$$

where

$$G_1 = \begin{bmatrix} 0 & 1 & 0 & 0 & 0 \\ -1 & 0 & 0 & 0 & 0 \\ 0 & 0 & 0 & 0 & 0 \\ 0 & 0 & 0 & 0 & 0 \\ 0 & 0 & 0 & 0 & 0 \end{bmatrix}.$$

The dynamics of the DC-link voltage in the presence of m DGR sets can be written as:

$$\dot{v}_{dc} = \frac{1}{C}\left(\beta_{rec_1}\sqrt{I_{G_1}^T G_2 I_{G_1}} + \cdots + \beta_{rec_m}\sqrt{I_{G_m}^T G_2 I_{G_m}} + D i_L - i_{load}\right), \tag{16}$$

where

$$G_2 = \begin{bmatrix} 1 & 0 & 0 & 0 & 0 \\ 0 & 1 & 0 & 0 & 0 \\ 0 & 0 & 0 & 0 & 0 \\ 0 & 0 & 0 & 0 & 0 \\ 0 & 0 & 0 & 0 & 0 \end{bmatrix}.$$

As a result, the overall dynamics of the energy generation side can be described using the following equations:

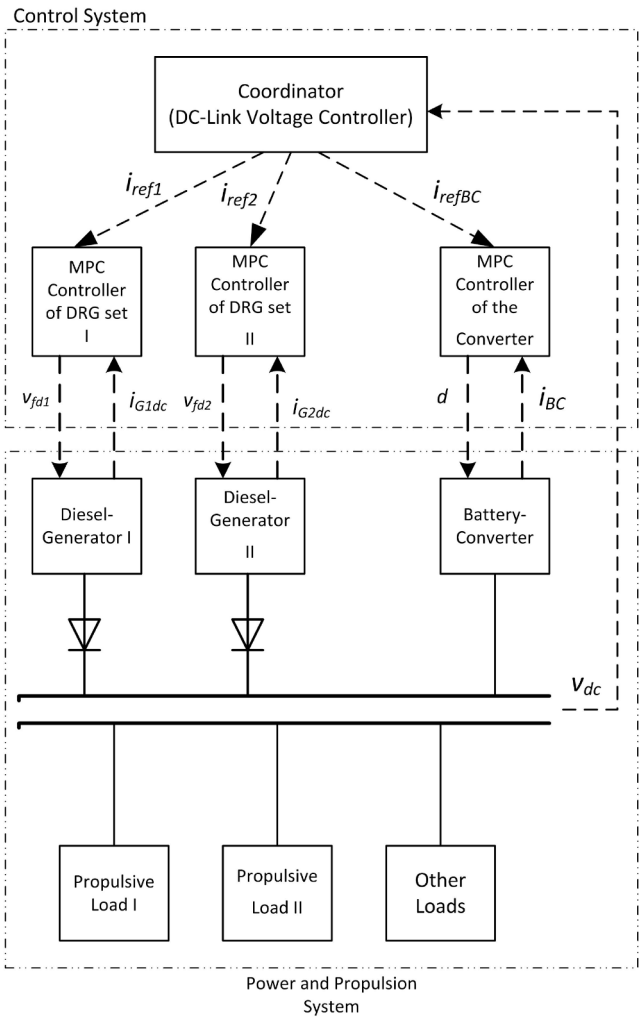

Fig. 3. The block diagram of the proposed control approach.

$$\begin{aligned} \dot{I}_{G_1} &= X_{G_1}^{-1} S_\omega(\omega_{dg_1}) X_{G_1} I_{G_1} + X_{G_1}^{-1} R_{G_1} I_{G_1} + v_{dc} X_{G_1}^{-1} E_1 + X_{G_1}^{-1} b v_{fd_1} \dot{\omega}_{dg_1} = \frac{1}{2H_1}(Q_{en_1} - I_{G_1}^T X_{G_1}^T G_1 I_{G_1}) \dot{Q}_{en_1} = -\frac{Q_{en_1}}{\tau_{s_1}} + K_{en_1} f_{en_1} : \dot{I}_{G_m} \\ &= X_{G_m}^{-1} S_\omega(\omega_{dg_m}) X_{G_m} I_{G_m} + X_{G_m}^{-1} R_{G_m} I_{G_m} + v_{dc} X_{G_m}^{-1} E_m + X_{G_m}^{-1} b v_{fd_m} \dot{\omega}_{dg_m} = \frac{1}{2H_m}(Q_{en_m} - I_{G_m}^T X_{G_m}^T G_1 I_{G_m}) \dot{Q}_{en_m} = -\frac{Q_{en_m}}{\tau_{s_m}} + K_{en_m} f_{en_m} \\ \dot{i}_L &= \frac{d}{L} v_{dc} - \frac{v_b(t)}{L} \dot{v}_{dc} \\ &= \frac{1}{C}\left(\beta_{rec_1}\sqrt{I_{G_1}^T G_2 I_{G_1}} + \cdots + \beta_{rec_m}\sqrt{I_{G_m}^T G_2 I_{G_m}} + D i_L - \frac{P}{v_{dc}}\right), \end{aligned} \tag{17}$$

where

$$E_j = \begin{bmatrix} \alpha_{rec_j} \sin(\arctan(\frac{i_{d_j}}{i_{q_j}}) - \phi_{rec_j}) \\ \alpha_{rec_j} \cos(\arctan(\frac{i_{d_j}}{i_{q_j}}) - \phi_{rec_j}) \\ 0 \\ 0 \\ 0 \end{bmatrix}. \tag{18}$$

In (17), the system outputs are $\omega_{dg_1}, \ldots, \omega_{dg_m}$, and v_{dc}, which must be controlled. The system inputs are $v_{fd_1}, \ldots, v_{fd_m}, f_{en_1}, \ldots, f_{en_m}$, and d.

In the next section, an MPC-based multi-level control approach is proposed involving a coordinating controller on the top level which derives the overall required DC current to keep the voltage around its nominal point. The low level modules control the DC current generation. For the design of this control approach, the model in (17) is employed for both high and low level controllers.

3. Proposed control strategy

In this section, the proposed two-level control approach is explained. This strategy is based on determining the required current by a supervisory controller to keep the DC voltage at its nominal value and then, providing the current by controlling the DC current output of the energy sources, i.e., DGR sets and the battery-converter set.

In this section, first, the control approaches for the low level controllers are presented. These modules are responsible for controlling the DC current generated by the energy sources, i.e., DGR sets and the battery-converter set. For this aim, an MPC accompanied by an IOFL scheme is adopted. Then, the higher control level is discussed which aims at determining a feasible desired DC current that should be generated by the energy sources. A schematic diagram of the overall control approach is shown in Fig. 3.

3.1. Control of the DGR sets

In this part, the proposed approach for the control of DGR sets is explained. From Eq. (17), the mathematical model of DGR set j is:

$$\begin{aligned}
\dot{I}_{\mathrm{G_j}} = \;& X_{\mathrm{G_j}}^{-1} S_{\omega}(\omega_{\mathrm{dg_j}}) X_{\mathrm{G_j}} I_{\mathrm{G_j}} + X_{\mathrm{G_j}}^{-1} R_{\mathrm{G_j}} I_{\mathrm{G_j}} \\
& + v_{dc} X_{\mathrm{G_j}}^{-1} E_j + X_{\mathrm{G_j}}^{-1} b v_{\mathrm{fd_j}} \\
\dot{\omega}_{\mathrm{dg_j}} = \;& \frac{1}{2H_j}(Q_{\mathrm{en_j}} - I_{\mathrm{G_2}}^T X_{\mathrm{G_j}}^T G_j I_{\mathrm{G_j}}) \\
\dot{Q}_{\mathrm{en_j}} = \;& -\frac{Q_{\mathrm{en_j}}}{\tau_{\mathrm{s_j}}} + K_{\mathrm{en_j}} f_{\mathrm{en_j}},
\end{aligned} \tag{19}$$

where $y_1^j = \omega_{\mathrm{dg_j}}$ and $y_2^j = I_{\mathrm{Gjdc}} = \beta_{\mathrm{rec_j}} \sqrt{I_{\mathrm{G_j}}^T G_2 I_{\mathrm{G_j}}}$ are the outputs to be controlled by the controller. The system inputs are $f_{\mathrm{en_j}}$ and $v_{\mathrm{fd_j}}$. The overall number of states is $n = 7$ with generator j's currents $I_{\mathrm{G_j}}$, diesel-generator shaft speed $\omega_{\mathrm{dg_j}}$, and diesel engine torque $Q_{\mathrm{en_j}}$ being the states of the system.

The above system can be represented as:

$$\begin{aligned}
\dot{x}_j &= f_j(x) + \sum_{i=1}^{2} g_i^j(x) u_i^j \\
y_i^j &= h_i^j(x) \qquad i = 1, 2,
\end{aligned} \tag{20}$$

where x_j is the vector of states and u_1^j and u_2^j are the system inputs. Function $f_j : \mathbb{R}^7 \to \mathbb{R}^7$ is the state transition function. Moreover, $g_1^j(x) = [X_{G_j}^{-1} b, 0, 0]^T, g_2^j(x) = [0, 0, K_{\mathrm{en_j}}]^T$.

System (19) is said to be input-output feedback linearizable if the vector of relative degrees exists [43]. By applying the Lie derivative to the system outputs, the decoupling matrix is calculated as:

$$\Delta(x_j) = \begin{bmatrix} \frac{1}{H_j} I_{\mathrm{G_j}}^T X_{\mathrm{G_j}}^T G_1 X_{\mathrm{G_j}}^{-1} b & \frac{K_{\mathrm{en_j}}}{2H_j} \\ \frac{I_{\mathrm{G_j}}^T G_2 X_{\mathrm{G_j}}^{-1} b}{\sqrt{I_{\mathrm{G_j}}^T G_2 I_{\mathrm{G_j}}}} & 0 \end{bmatrix}, \tag{21}$$

with $\{2, 1\}$ as the vector of relative degrees. Note that the above matrix is nonsingular around the operating points of the system. As a result, a nonlinear coordinate transformation can be established by choosing the first $r = r_1 + r_2 = 3$ coordinates as:

$$\zeta_l^i = \Phi_l^i(x_j) = L_{f_j}^{i-1} h_l(x_j), \tag{22}$$

with non-negative integers $i \in \{1, 2\}$ and $l \in \{1, 2\}$. The other additional $n - r$ coordinates can be found such that $\Phi_j(x_j)$ is invertible [43]. In general, the normal form of the transformed partially linear system is:

$$\begin{aligned}
\dot{\zeta}_1^1 &= \zeta_1^2 \\
\dot{\zeta}_1^2 &= v_1 = L^2_{(f_j + g_1^j u_1^j + g_2^j u_2^j)} h_1^j(x) \\
\dot{\zeta}_2^1 &= v_2^j = L^1_{(f_j + g_1^j u_1^j + g_2^j u_2^j)} h_2^j(x_j) \\
\dot{\eta}_j &= q(\zeta_j, \eta_j) \\
y_1^j &= \zeta_1^1 \\
y_2^j &= \zeta_2^1,
\end{aligned} \tag{23}$$

where v_1 and v_2 are the system inputs for the transformed linear systems. Vector of nonlinear functions q represents zero-dynamics/internal dynamics where its elements are chosen using the condition:

$$L_{g_j} \Phi_{r+i}(x) = 0, \tag{24}$$

where $1 \leqslant i \leqslant 4$ and $1 \leqslant j \leqslant 2$. After calculation, we have:

$$\begin{aligned}
\zeta_1^1 &= \omega_{\mathrm{dg_j}} \\
\zeta_1^2 &= \frac{1}{2H_j}(Q_{\mathrm{en_j}} - I_{\mathrm{G_2}}^T X_{\mathrm{G_j}}^T G_j I_{\mathrm{G_j}}) \\
\zeta_2^1 &= \beta_{\mathrm{rec_j}} \sqrt{I_{\mathrm{G_j}}^T G_2 I_{\mathrm{G_j}}}.
\end{aligned}$$

The relationship between the original system inputs u_1^j and u_2^j with inputs of the transformed system can be written as:

$$\begin{bmatrix} u_1^j \\ u_2^j \end{bmatrix} = -\Delta^{-1}(x_j) \left(\begin{bmatrix} L_{f_j}^2 y_1^j \\ L_{f_j}^1 y_2^j \end{bmatrix} + \begin{bmatrix} v_1^j \\ v_2^j \end{bmatrix} \right). \tag{25}$$

Then, the decoupled linear systems are defined as:

$$\begin{bmatrix} \dot{\zeta}_1^1 \dot{\zeta}_1^2 \end{bmatrix} = \begin{bmatrix} 0 & 1 \\ 0 & 0 \end{bmatrix} \begin{bmatrix} \zeta_1^1 \\ \zeta_1^2 \end{bmatrix} + \begin{bmatrix} 0 \\ 1 \end{bmatrix} v_1^j \qquad \dot{\zeta}_2^1 = v_2^j. \tag{26}$$

To control the DGR set two MPC problems should be solved; one for the speed control and the second one for the current generation control.

After discretization, the following MPC problem is defined for controlling the speed of the diesel-generator.

$$\mathbb{P}_1^j(\zeta_1^1) : \min_{v_1^j} \left(V_{\mathrm{N}}(\zeta_1^1, v_1^j) = \sum_{i=k}^{k+N-1} S\left(\zeta_1^1(i), \omega_{\mathrm{ref}}^j(i), v_1^j(i)\right) + S_{\mathrm{f}}\left(\zeta_1^1(k+N)\right) \right) \tag{27}$$

subject to (26) with:

$$\begin{aligned}
& \zeta_{1_{\min}}^1 \leqslant \zeta_1^1(k+i) \leqslant \zeta_{1_{\max}}^1 \\
& v_{1_{\min}}^j(k+i-1) \leqslant v_1^j(k+i-1) \leqslant v_{1_{\max}}^j(k+i-1) \\
& \forall i \in [0, N],
\end{aligned} \tag{28}$$

where $V_{\mathrm{N}}(.)$ is the MPC cost function, N is the prediction horizon, k is the discrete time step of the system with sample time T_{dc}^j and $S_{\mathrm{f}}(.)$ is the terminal cost defined as:

$$S_{\mathrm{f}}\left(z_2^1(N)\right) = \left(\zeta_1^1(N) - \omega_{\mathrm{ref}}^j(N)\right)^2. \tag{29}$$

Moreover,

$$S\left(\zeta_1^1(k), \omega_{\mathrm{ref}}^j(k), v_1^j(k)\right) = \alpha\left(\zeta_1^1(k) - \omega_{\mathrm{ref}}^j(k)\right)^2 + \beta v_1^j(k)^2, \tag{30}$$

where non-negative parameters α and β are weight factors.

Similar to the diesel-generator speed control, the following MPC problem is defined for the generated DC current control of DGR set j:

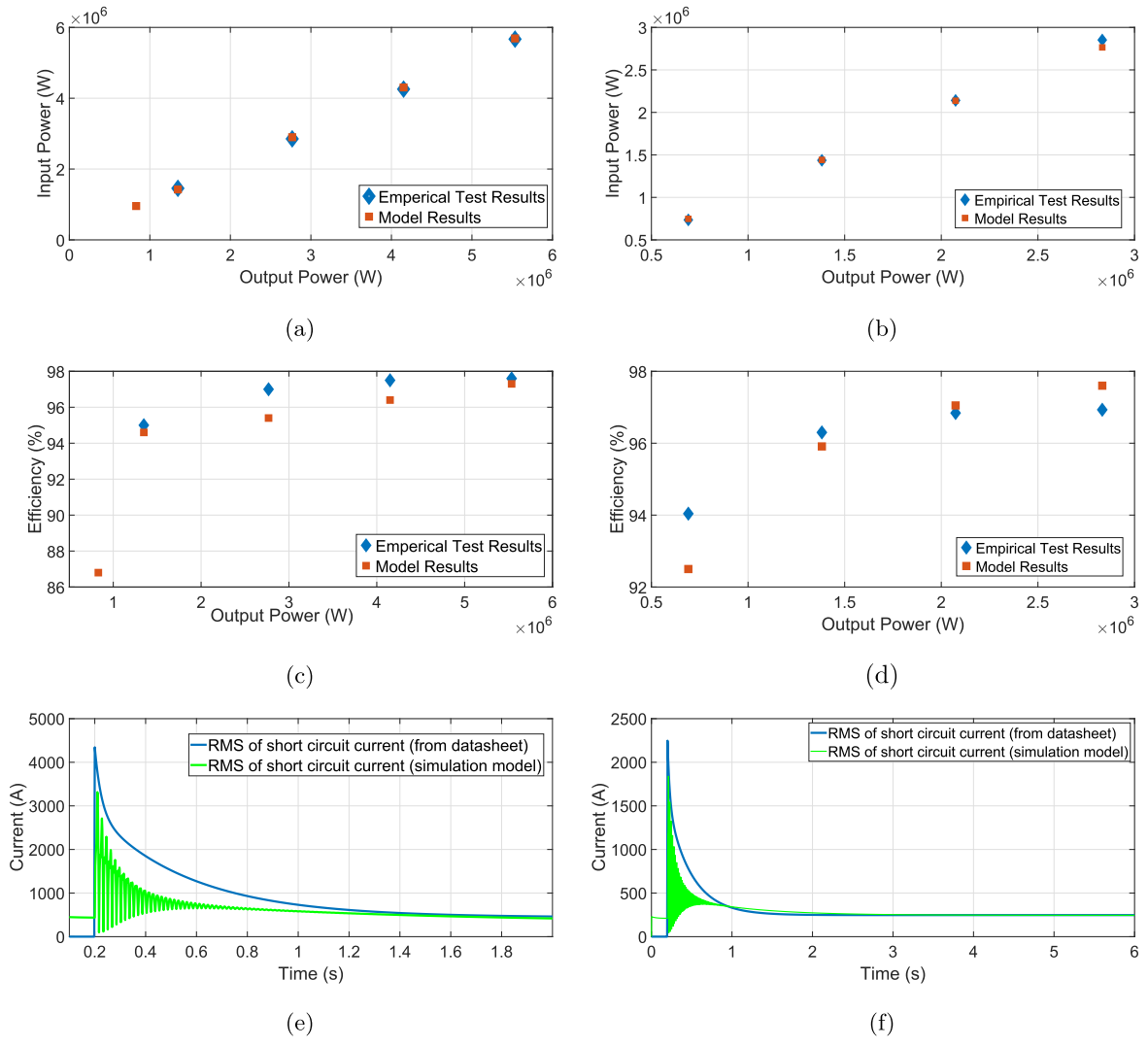

Fig. 4. Synchronous generators model validation: simulation model results vs. emperical test results. (a), (b) The relationship between input and output power of 6150 kW and 3456 kW generators, respectively. (c), (d) Efficiency at different loading conditions of 6150 kW and 3456 kW generators, respectively. (e), (f) Model and datasheet short circuit current comparison of 6150 kW and 3456 kW generators, respectively.

$$\mathbb{P}_2^j(\zeta_2^1) : \min_{v_2^j} \left(V_N(\zeta_2^1, v_2^j) = \sum_{i=k}^{k+N-1} S\left(\zeta_2^1(i), i_{j_{ref}}(i), v_2^j(i)\right) + S_f\left(\zeta_2^1(k+N)\right) \right) \tag{31}$$

subject to (26) with:

$$\begin{aligned} &\zeta_{2_{\min}}^1 \leqslant \zeta_2^1(k+i) \leqslant \zeta_{2_{\max}}^1 \\ &v_{2_{\min}}^j(k+i-1) \leqslant v_2^j(k+i-1) \leqslant v_{2_{\max}}^j(k+i-1) \\ &\forall i \in [0, N]. \end{aligned} \tag{32}$$

3.1.1. Constraint linearization

Although the systems in (26) are linear, due to the nonlinearity of constraints in (28) and (32), quadratic programming schemes cannot be used for solving the optimization problems in (27) and (31). In this part, by using the results in [29,30], a strategy is proposed to transform the nonlinear input constraints into linear constraints so that quadratic programming approaches are applicable.

The input constraints of the system cannot be found straightforward way since:

$$\begin{bmatrix} v_1^j \\ v_2^j \end{bmatrix} = \begin{bmatrix} \Psi_1^j(x_j, u_j) \\ \Psi_2^j(x_j, u_j) \end{bmatrix} = \Delta(x_j)u_j - \begin{bmatrix} L_{f_j}^2 y_1^j \\ L_{f_j} y_2^j \end{bmatrix}. \tag{33}$$

The problem with the exact mapping of constraints is that future values of states x_j and inputs u_1^j and u_1^j are not immediately available and should be found by solving a nonlinear optimization problem which employs predicted values of x_j over the horizon N. Obviously, this strategy is very time consuming and eliminates the advantages of adopting an MPC-based control strategy. However, the exact mapping of the future input constraints is impractical since $v_1^j(k+i)$ and $v_2^j(k+i), i \in [0, N]$ are not implemented. As a result, a strategy is adopted with which $v_{1_{\min}}^j(k+i)$, $v_{1_{\max}}(k+i)$, $v_{2_{\min}}^j(k+i)$, and $v_{2_{\max}}^j(k+i)$ are approximated over the prediction horizon and $v_{1_{\min}}^j(k), v_{1_{\max}}^j(k), v_{2_{\min}}^j(k)$, and $v_{2_{\max}}^j(k)$ represent exact values.

To this end, the following optimization problems are defined.

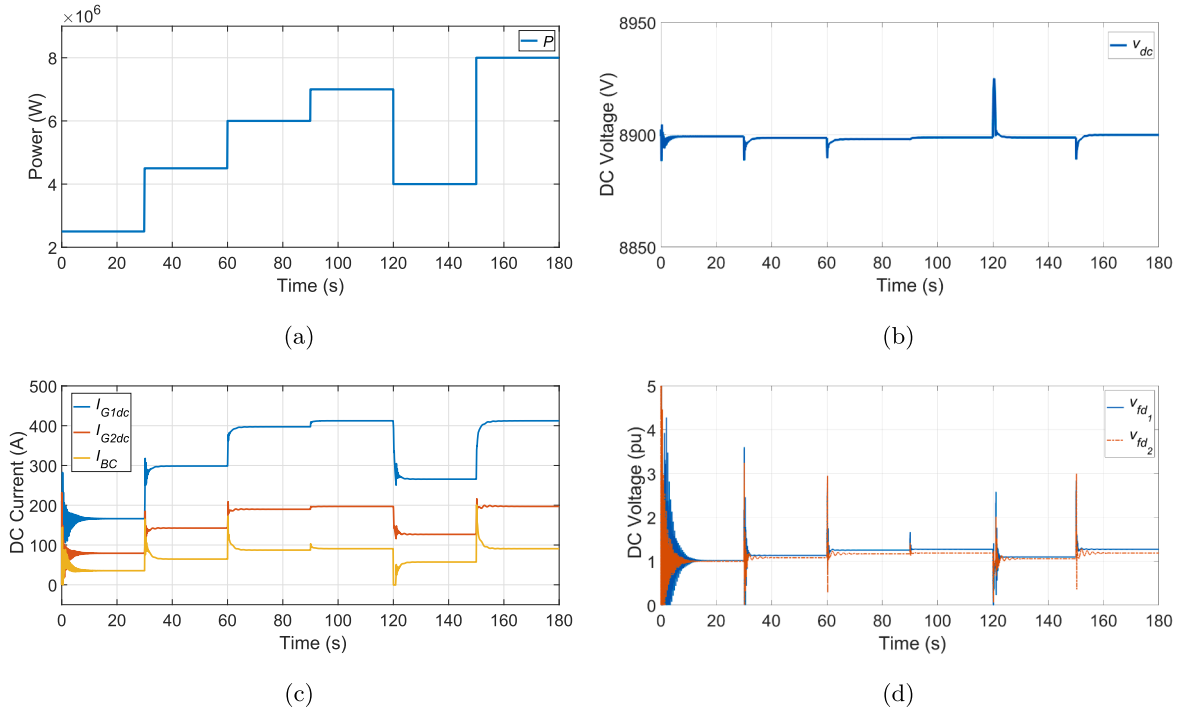

Fig. 5. DC-link voltage stability simulation results in Experiment I. (a) The varying load applied to the power system. (b) The DC-link voltage. (c) DC currents provided by the energy sources. (d) Field voltage of the synchronous.

$$
\begin{aligned}
v^j_{1_{\min}}(k+i-1) &= \min_{v^j_1(k+i-1)} \Psi^j_1 \quad \left(x_j(k), u^j(k+i-1)\right)\\
v^j_{1_{\max}}(k+i-1) &= \max_{v^j_1(k+i-1)} \Psi^j_1 \quad \left(x_j(k), u^j(k+i-1)\right)\\
v_{2_{\min}}(k+i-1) &= \min_{v^j_2(k+i-1)} \Psi^j_2 \quad \left(x_j(k), u^j(k+i-1)\right)\\
v_{2_{\max}}(k+i-1) &= \max_{v_2(k+i-1)} \Psi^j_2 \quad \left(x_j(k), u^j(k+i-1)\right)\\
&\forall i \in [0, N].
\end{aligned} \tag{34}
$$

Solving the above problem is straightforward as $x_j(k)$ is known and $u^j(k+i-1)$ appears linearly in functions $\Psi^j_1(.)$ and $\Psi^j_2(.)$. Using the above equation, it is guaranteed that the implemented control action is within the exact constraints of the actual system. Furthermore, finding the input variable bounds for the rest of the horizon is computationally trivial if (47) is adopted.

3.2. Control of the battery-converter set

In this part, the objective is to control the DC current generated by the battery-converter set. To this end, and in order to handle constraints and utilize the prediction of the required propulsive load, an MPC approach is proposed.

As mentioned, in this paper, a non-isolated converter model is adopted for the DC/DC conversion stage.

The dynamical model of the converter is:

$$
\begin{aligned}
\dot{i}_{\mathrm{L}} &= \frac{d(t)}{L} v_{\mathrm{dc}}(t) - \frac{v_{\mathrm{b}}(t)}{L}\\
i_{\mathrm{BC}} &= D i_{\mathrm{L}},
\end{aligned} \tag{35}
$$

where d is the control input and i_{BC} is the output. The relationship between the input and output is linear, if v_{dc} is constantly measured and kept constant around its nominal value. Note that changes in v_{b} are very slow and negligible.

To control i_{BC}, the following MPC problem is defined:

$$
\begin{aligned}
\mathbb{P}_{\mathrm{BC}}(i_{\mathrm{BC}}) : \min_{d} (V_{\mathrm{N}}(i_{\mathrm{BC}}, d) = &\sum_{i=k}^{k+N-1} S\big(i_{\mathrm{BC}}(i), I_{BC_{\mathrm{ref}}}(i), d(i)\big)\\
&+ S_{\mathrm{f}}(i_{\mathrm{BC}}(k+N))\big)
\end{aligned} \tag{36}
$$

subject to (35) and

$$
\begin{aligned}
&I_{BC_{\min}} \leqslant \zeta^1_1(k+i) \leqslant I_{BC_{\max}}\\
&0 \leqslant d(k+i-1) \leqslant 1\\
&\forall i \in [0, N].
\end{aligned} \tag{37}
$$

3.3. Coordinator: Control for the DC-link voltage

In this section, the high level control approach is presented. This module is responsible for determining a current with which the DC voltage is kept around its nominal value:

The dynamics of the DC-link can be represented as

$$
\dot{v}_{\mathrm{dc}} = \frac{1}{C}(I_{\mathrm{G1dc}} + \ldots m + I_{\mathrm{Gmdc}} + i_{\mathrm{BC}} - \frac{P}{v_{\mathrm{dc}}}) = \frac{1}{C}(i_{\mathrm{dc}} - \frac{P}{v_{\mathrm{dc}}}), \tag{38}
$$

where i_{dc} is considered as the system input and v_{dc} is the system output.

Let the solution of controlling v_{dc} be $i_{\mathrm{ref}_{\mathrm{dc}}}$. Note that, in reality, there is no active controller at the rectification stage and $i_{\mathrm{ref}_{\mathrm{dc}}}$ is provided by the energy sources. However, $i_{\mathrm{ref}_{\mathrm{dc}}}$ can not be exactly tracked by i_{dc}. This tracking error is formulated as:

$$
e_{i_{\mathrm{dc}}} = i_{\mathrm{ref}_{\mathrm{dc}}} - i_{\mathrm{dc}}. \tag{39}
$$

Due to the correctness of control methods presented in Sections 3.1 and 3.2, $e_{i_{\mathrm{dc}}}$ is bounded. Therefore, (38) can be written as:

$$
\dot{v}_{\mathrm{dc}} = \frac{1}{C}(i_{\mathrm{ref}_{\mathrm{dc}}} - \frac{P}{v_{\mathrm{dc}}} + e_{i_{\mathrm{dc}}}), \tag{40}
$$

where $i_{\mathrm{ref}_{\mathrm{dc}}}$ is regarded as the system input and $e_{i_{\mathrm{dc}}}$ as a bounded additive disturbance. Due to the presence of a CPL, the above system has nonlinear dynamics. In order to control this system, similarly as in

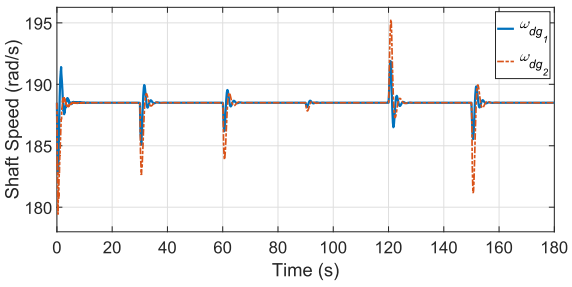

(a) Shaft speed of diesel-generators.

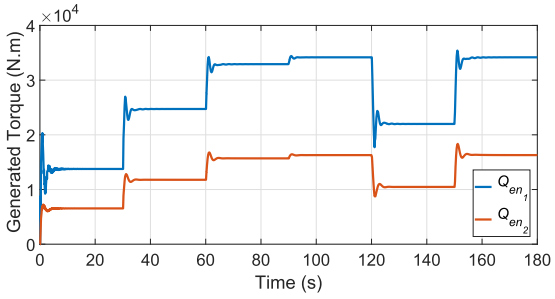

(b) Diesel engine torques.

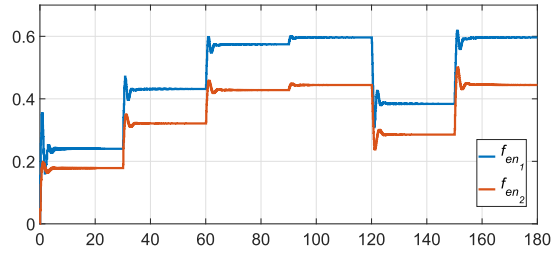

(c) Fuel index of the diesel engines.

Fig. 6. Diesel-generators performance (Experiment I).

Section 3.1, an auxiliary control input is defined for establishing a linear relationship between system input and output as:

$$\nu_{\mathrm{i}} = \frac{1}{C}(i_{\mathrm{ref_{dc}}} - \frac{P}{v_{\mathrm{dc}}}), \tag{41}$$

which leads to the following transformed system:

$$\dot{v}_{\mathrm{dc}} = \nu_{\mathrm{i}} + \frac{e_{\mathrm{i_{dc}}}}{C}. \tag{42}$$

To control (42), based on the results in [28], a robust tube-based MPC approach is proposed. This approach is based on extracting a trajectory for a nominal system and then, by adopting a linear control law, the trajectory of the system is steered towards the trajectory of the nominal system. The nominal system is defined as:

$$\dot{z}_{\mathrm{dc}} = \tau_{\mathrm{dc}}, \tag{43}$$

where z_{dc} is the state and τ_{dc} is the system input. To generate the nominal trajectory, the following MPC problem is defined:

$$\begin{aligned}\mathbb{P}_{\mathrm{DC}}(z_{\mathrm{dc}}) : \min_{d}(V_{\mathrm{N}}(z_{\mathrm{dc}}, \tau_{\mathrm{dc}}) = \sum_{i=k}^{k+N-1} S\big(z_{\mathrm{dc}}(i), v_{\mathrm{dc_{ref}}}(i), \tau_{\mathrm{dc}}(i)\big) \\ + S_{\mathrm{f}}(z_{\mathrm{dc}}(i)(k+N))\big),\end{aligned} \tag{44}$$

subject to (43) with:

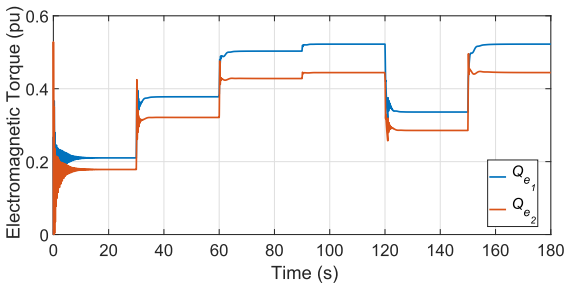

(a) Electromagnetic torque of the synchronous generators.

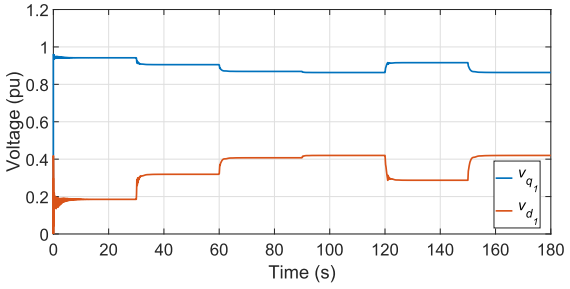

(b) dq voltages of the first synchronous generators.

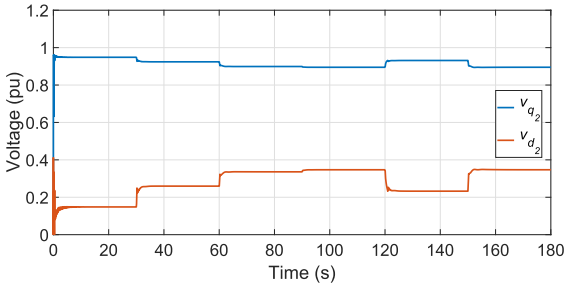

(c) dq voltages of the second synchronous generators.

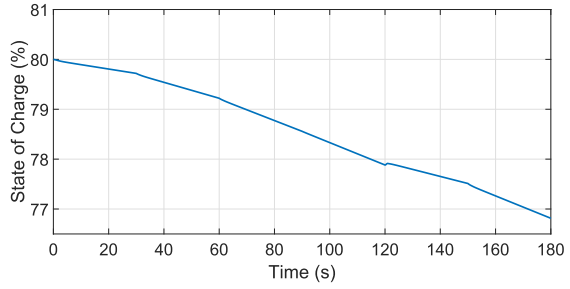

(d) The SOC of the battery during simulation.

Fig. 7. Performance of synchronous generators and the battery in Experiment I.

$$\begin{aligned}&z_{\mathrm{dc_{min}}} \leqslant z_{\mathrm{dc}}(k+i) \leqslant z_{\mathrm{dc_{max}}} \\ &\tau_{\mathrm{dc_{min}}}(k+i-1) \leqslant \tau_{\mathrm{dc}}(k+i-1) \leqslant \tau_{\mathrm{dc_{max}}}(k+i-1) \\ &\forall i \in [0, N].\end{aligned} \tag{45}$$

To steer the actual system's trajectory towards the trajectory of the nominal system, the following control rule is defined:

$$\nu_{\mathrm{i}}(t) = \kappa_{\mathrm{dc}}(z_{\mathrm{dc}}(t)) + K_{\mathrm{dc}}(v_{\mathrm{dc}}(t) - z_{\mathrm{dc}}(t)) \tag{46}$$

where $\kappa_{\mathrm{dc}}(.)$ is the solution of the MPC problem in (44) and $K_{\mathrm{dc}} \leqslant 0$ is the feedback gain.

Similar to Section 3.1, the constraints in (45) are found by solving the following optimization problems:

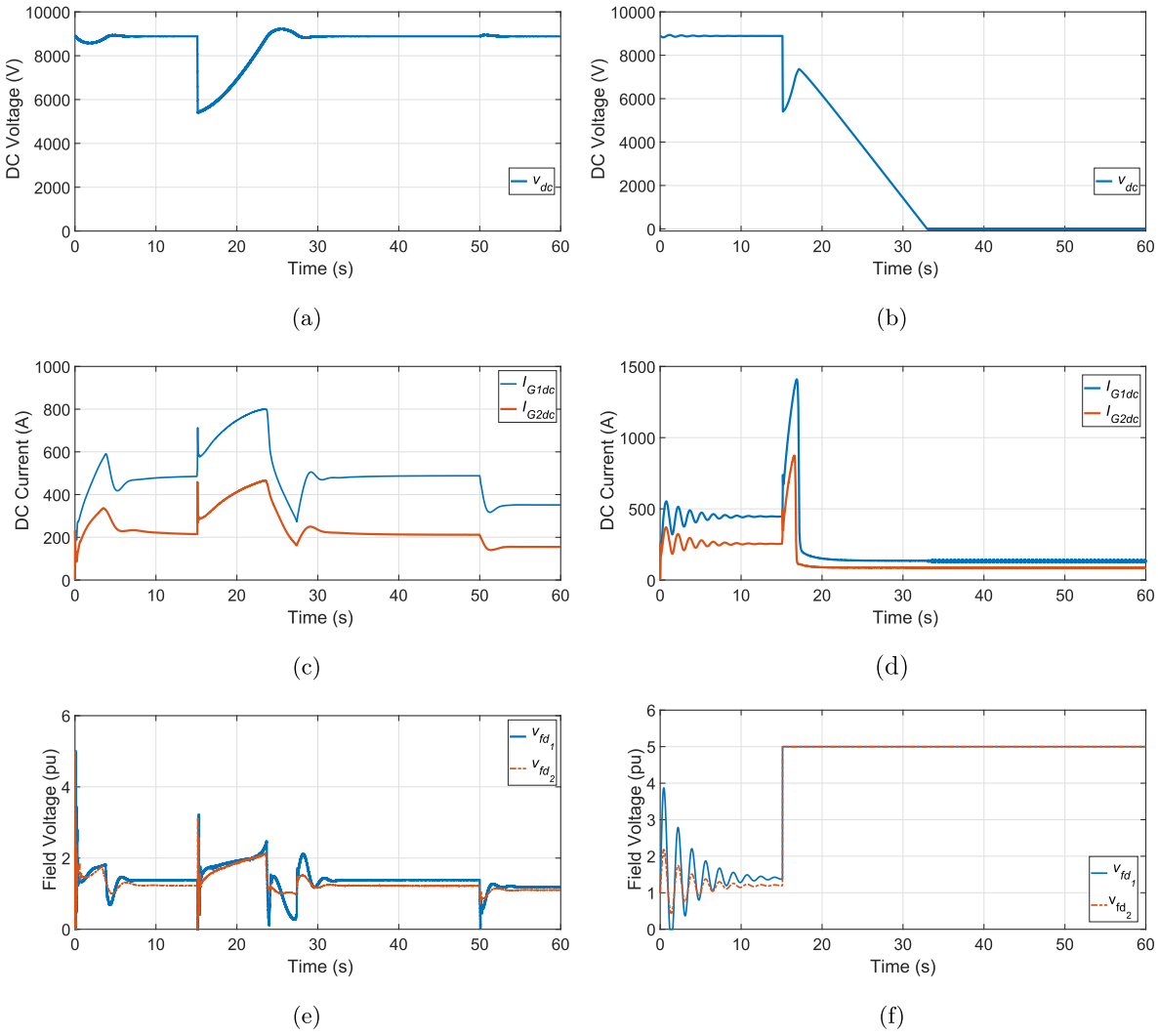

Fig. 8. Short circuit experiment results using the proposed MPC-based approach vs. the conventional droop PID-based approach. (a) DC-link voltage response using the proposed approach. (b) DC-link voltage response using the conventional PID-based approach. (c) Generated currents by the energy sources using the proposed approach. (d) Generated currents by the energy sources using theconventional PID-based approach. (e) Field voltage of the synchronous generators (the proposed approach). (f) Field voltage of the synchronous generators (the conventional PID-based approach).

$$\begin{aligned}\tau_{\mathrm{dc}_{\min}}(k+i-1) &= \min_{i_{\mathrm{ref}_{\mathrm{dc}}}(k+i-1)} \nu_{\mathrm{i}} \quad \left(v_{\mathrm{dc}}(k), i_{\mathrm{ref}_{\mathrm{dc}}}(k+i-1)\right)\\ \tau_{\mathrm{dc}_{\max}}(k+i-1) &= \max_{i_{\mathrm{ref}_{\mathrm{dc}}}(k+i-1)} \nu_{\mathrm{i}} \quad \left(v_{\mathrm{dc}}(k), i_{\mathrm{ref}_{\mathrm{dc}}}(k+i-1)\right)\\ &\quad \forall i \in [0, N].\end{aligned} \tag{47}$$

Note that the bounds on the input variables can be considered tighter [28].

Remark 1. The relationship between the maneuvering controller and the proposed power generation control approach is established in a similar way as in the methodology proposed in [26] where an MPC control approach is used for maneuvering control. Through the model of propellers and efficiency curves of induction motor, the propulsive load is predicted. As a result, $P(k), P(k+1), \ldots, P(k+N)$ are realizable.

Remark 2. The integration of the energy management module and the power generation controller is established by sharing the reference current $i_{\mathrm{ref}_{\mathrm{dc}}}$ between the energy sources as:

$$i_{\mathrm{ref}_{\mathrm{dc}}} = \xi_{\mathrm{DGR}_1} i_{\mathrm{ref}_{\mathrm{dc}}} + \ldots + \xi_{\mathrm{DGR}_m} i_{\mathrm{ref}_{\mathrm{dc}}} + \xi_{\mathrm{BC}} i_{\mathrm{ref}_{\mathrm{dc}}}, \tag{48}$$

where $i_{\mathrm{ref}_1} = \xi_{\mathrm{DGR}_1} i_{\mathrm{ref}_{\mathrm{dc}}}$, …, $i_{\mathrm{ref}_m} = \xi_{\mathrm{DGR}_m} i_{\mathrm{ref}_{\mathrm{dc}}}$, and $i_{\mathrm{ref}_1} = \xi_{\mathrm{BC}} i_{\mathrm{ref}_{\mathrm{BC}}}$.

4. Simulation experiments

In this part, the performance of the proposed control approach is evaluated through simulation experiments. First, the simulation model is discussed and then, the experiment results are presented. For evaluating the performance of the proposed approach, two simulation-based experiments are considered:

1. Voltage control under a CPL load with varying power over time.
2. Short circuit experiment under a CPL.

4.1. Simulation model validation

The simulation model is established based on the component models that are provided by ShipDrive project partner Damen Schelde Naval Shipbuilding. The overall energy generation side can deliver 10606 kW, provided by two DGR sets and a battery-converter set. In order to show better the applicability and flexibility of the control approach to different component models, two non-similar diesel-generators are considered for the energy generation side. These diesel-generators have different power ratings and dynamical model parameters. The first

diesel-generator is a 6150 kW, 6600 V, 60 Hz and the second one is a 3456 kW, 6600 V, 60 Hz. Both models represent existing diesel-generators.

Based on the standard per-unit (pu) parameters, the fundamental models of the generators are extracted. Then, the models are validated using performance data of generators. The validation results are illustrated in Fig. 4. The empirical test results are compared with the results of the models in this paper. For this purpose, the generators are connected to a three phase load. The results indicate high accuracy of the model, with less than 1.5% error for different output powers.

The comparison of the Root-Mean-Square (RMS) value of the short circuit current and the computed short circuit current (based on the datasheet) are shown in Figs. 4e and 4f. The results indicate sufficient accuracy of the synchronous generator transients.

For the experiments in this section, two diesel engines with different specs are considered. The diesel engine of the larger synchronous generator can deliver 5.4 MW of power with twelve cylinders and gear ration 1/2. The other one is a 3.5 MW diesel engine with twelve cylinders and 1/2 gear ratio. For the voltage conversion stages, an average rectifier model with 96% of efficiency is considered. Moreover, a 1 MWh battery is considered with internal resistance of 0.01 ohm. The bidirectional converter data is provided in Appendix A.

The experiments are carried out on a PC with 2.8 GHz Intel Core i7-7600U CPU and 8 GB RAM. The MATLAB® 2018a Simscape toolbox is partially used for the development of the model.

4.2. Experiment I: Voltage control under varying CPL load

In this experiment, a CPL with varying power P over time is applied to the system. Both DGR sets and the battery-converter set are online and providing power. The power splits between energy sources are $\xi_{\mathrm{DGR}_1} = 0.6, \xi_{\mathrm{DGR}_2} = 0.3$, and $\xi_{\mathrm{BC}} = 0.1$. The load applied to the power system is shown in Fig. 5a.

It is assumed that the prediction horizon of the model predictive controller of the coordinator is $N = 20$ with sampling time $T_{\mathrm{dc}} = 0.1$s. Similar setting is used for the DC current controllers of the DGR sets and the converter. For the diesel-generators shaft speed control, the controller's prediction horizon are is as $N_{\omega} = 10$.

The simulation results of the voltage stability are shown in Figs. 5. It is shown that the energy sources respond actively to the load changes and as a result, the voltage stays around its nominal value. Moreover, the power splits between different sources stays around the desired values. The simulation results of the mechanical variables are shown in Fig. 6. It is shown that the shaft speed of diesel-generators are kept around the desired value by injecting feasible amount of fuel. The response of the engine torque is shown in Fig. 6b, representing the load changes during the simulation time. The simulation results of the synchronous generator's electrical variables are presented in Fig. 7. The SOC of the battery is shown in Fig. 7d.

4.3. Experiment II: Short circuit test

In this section, the tolerance of the proposed control approach is evaluated against a short circuit fault. Moreover, the performance of the two-level MPC controller is compared with the conventional droop control methods.

A 7.5 MW CPL is considered as a load that drops to 4.5 MW at $t = 50$ s. The DC-link short circuit fault happens at $t = 15.1$ s and stops at $t = 15.15$ s. Similar settings are considered for the proposed two-level MPC controller.

The simulation results are presented in Figs. 8a, 8c, and 8e. It is shown that the DC-link voltage can recover after the short circuit. This happened by increasing the generated DC current by the controllers. Fig. 8e, represents the controllers effort to keep the DC-link voltage stable.

This experiment is also carried out using conventional droop control approach. In this approach, the diesel-generator controllers are PI-based. For voltage regulation, the PI values of the first synchronous generator are $K_{\mathrm{P}_1} = 294.75$ and $K_{\mathrm{I}_1} = 2.3$. For the second synchronous generator, these values are $K_{\mathrm{P}_2} = 121.1$ and $K_{\mathrm{I}_2} = 2.9$. The PI values are estimated by using the transient time constant of the synchronous generators and the rough estimation of relationships between $v_{\mathrm{fd}_{1,2}}$ and the terminal voltages of the generators [42]. The simulation results of PI-based droop control scheme are shown in Figs. 8b, 8d, and 8f which indicate the failure of the control approach as after the short circuit incident, the voltage cannot be recovered.

5. Conclusions and future research

In this paper, a multi-level model predictive power generation control approach is proposed for DC Power and Propulsion Systems (DC-PPS). The objective is guaranteeing the stability of the system through keeping the DC voltage of the grid and shaft speed of diesel-generator sets around their nominal values. To develop the control approach, first a state space model for the on-board DC power system is established which captures the dynamics of the all on-board energy sources as well as rectifiers and the bidirectional converter. The control approach consists of a coordinator which acts as an artificial controller to determine the required DC current to keep the voltage around its nominal value and low level controllers that control the generated DC current by each prime mover set as well as the shaft speed of the diesel-generators. Input-Output Feedback Linearization (IOFL) as well as a technique to linearize the constraints is adopted to enable the use of quadratic programming approaches for solving the optimization problem of the model predictive controllers. The proposed control approach is evaluated through several simulation experiments on a high voltage DC-PPS with high fidelity component models that are provided by Damen Schelde Naval Ship Building. The advantages of using the proposed control approach can be summarized as:

- Unlike conventional droop control approaches, explicitly controlling the DC-link voltage through controlling the DC current generated by different energy sources.
- Enabling the use of quadratic programming approaches for solving the optimization problem of model predictive controllers by using IOFL and constraint linearization approaches.
- Straightforward interaction with energy management and maneuvering control modules.
- Suitable for the addition of other novel energy sources such as fuel cells and photovoltaics that are DC power sources.

The results of this paper lead to taking a step towards a more effective energy conversion and preservation strategy in the maritime industry. These results can also be extended to other domains such as stability of power grids, control of AC and DC microgrids, and power generation control in the presence of renewable energy sources. Moreover, they indicate the viability of Model Predictive Control (MPC)-based approaches for dealing with on-board power generation and stability issues.

The effect of non-propulsive loads is quite dominant in the case of vessels with large hotels and several facilities on-board such as naval vessels, cruise ships, support vessels, and pipe laying vessels. These loads create great uncertainty in the power demand. Moreover, they influence the stability of the power system and necessitate the existence of sophisticated fault-detection and isolation approaches. Future research in the context of this work invlolves the non-propulsive loads as well as the integration of other new energy sources (such as fuel cells) in relation to power generation control. Furthermore, based on the analysis and conclusions in [44], fault-detection and isolation schemes for DC-PPS will be investigated.

CRediT authorship contribution statement

Ali Haseltalab: Conceptualization, Data curation, Formal analysis, Investigation, Methodology, Software, Validation, Writing – original draft. **Faisal Wani:** Conceptualization, Formal analysis, Methodology, Writing – review & editing. **Rudy R. Negenborn:** Conceptualization, Funding acquisition, Project administration, Methodology, Writing – review & editing.

Declaration of Competing Interest

The authors declare that they have no known competing financial interests or personal relationships that could have appeared to influence the work reported in this paper.

Acknowledgment

The authors thank the Research and Development department of Damen Schelde Naval Shipbuilding, especially Piet Lievense, for providing the power system component models and data.

This research is supported by the projects "ShipDrive: A Novel Methodology for Integrated Modelling, Control, and Optimization of Hybrid Ship Systems" (project 13276) and "GasDrive: Minimizing Emissions and Energy Losses at Sea with LNG Combined Primemovers, Underwater Exhausts and Nano Hull Materials" (project 14504) of the Netherlands Organization for Scientific Research (NWO), domain Applied and Engineering Sciences (TTW), and Researchlab Autonomous Shipping (RAS) of Delft University of Technology.

Appendix A. Specifications of the high voltage DC-PPS

- **The ship model:** Length: 90 m, deadweight at design draught: 425 ton, Displacement at design draught 2565 ton.
- **Induction motors:** 1.8 MW, 6600 V, 60 Hz, four poles.
- **Diesel Engine I:** $K_{\text{en}} = 57295$, twelve cylinders, 5.4 MW, diesel-generator gear ratio: $\frac{1}{2}$.
- **Diesel Engine II:** $K_{\text{en}} = 36668$, twelve cylinders, 3.5 MW, diesel-generator gear ratio: $\frac{1}{2}$.
- **Synchronous generator I:** 6.150 MW, 6600 v, 60 Hz, 10 poles, $H = 0.71, r_s = 0.0363, r_{\text{fd}} = 0.2, r_{\text{kd}} = 0.722, r_{\text{kq}} = 0.1072, L_{\text{d}} = 0.0323, L_{\text{md}} = 0.0305, L_{\text{kd}} = 0.0320, L_{\text{fd}} = 0.4820, L_{\text{q}} = 0.0163, L_{\text{mq}} = 0.0144$ and $L_{\text{kq}} = 0.0163$. Resistance values are in ohm and inductance values are in Henry.
- **Synchronous generator II:** 3.456 MW, 6600 v, 60 Hz, 10 poles, $H = 0.56, r_s = 0.0601, r_{\text{fd}} = 0.177, r_{\text{kd}} = 1.5049, r_{\text{kq}} = 0.1726, L_{\text{d}} = 0.05768, L_{\text{md}} = 0.05407, L_{\text{kd}} = 0.06125, L_{\text{fd}} = 0.3204, L_{\text{q}} = 0.02702, L_{\text{mq}} = 0.0144$ and $L_{\text{kq}} = 0.02341$. Resistance values are in ohm and inductance values are in Henry.
- **Rectifier:** Six-pulse rectifier, $\beta_{\text{rec}} = 0.981$.
- **DC-link:** $C = 0.5$ F.
- **Bidirectional Converter:** $L = 0.0005$H, $v_{\text{b}} = 1000$V.

References

[1] Zahedi B, Norum LE, Ludvigsen KB. Optimized efficiency of all-electric ships by dc hybrid power systems. J Power Sources 2014;255:341–54.
[2] Geertsma R, Negenborn R, Visser K, Hopman J. Design and control of hybrid power and propulsion systems for smart ships: A review of developments. Appl Energy 2017;194:30–54.
[3] Seenumani G, Peng H, Sun J. A reference governor-based hierarchical control for failure mode power management of hybrid power systems for all-electric ships. J Power Sources 2011;196(3):1599–607.
[4] Emadi A, Khaligh A, Rivetta CH, Williamson GA. Constant power loads and negative impedance instability in automotive systems: definition, modeling, stability, and control of power electronic converters and motor drives. IEEE Trans Veh Technol 2006;55(4):1112–25. July.
[5] Feng X, Butler-Purry K, Zourntos T. Multi-agent system-based real-time load management for all-electric ship power systems in dc zone level. IEEE Trans Power Syst 2012;27(4):1719–28. November.
[6] Haseltalab A, Botto MA, Negenborn RR. Model predictive dc voltage control for all-electric ships. Control Eng Pract 2019;90:133–47.
[7] den Broeck GV, Stuyts J, Driesen J. A critical review of power quality standards and definitions applied to dc microgrids. Appl Energy 2018;229:281–8.
[8] Gadoura I, Grigore V, Hatonen J, Kyyra J, Vallittu P, Suntio T. Stabilizing a telecom power supply feeding a constant power load. In: Proceedings of INTELEC - Twentieth International Telecommunications Energy Conference; Oct 1998. p. 243–8.
[9] Balog RS, Weaver WW, Krein PT. The load as an energy asset in a distributed DC smartgrid architecture. IEEE Trans Smart Grid 2012;3(1):253–60. March.
[10] Lu X, Sun K, Guerrero JM, Vasquez JC, Huang L, Wang J. Stability enhancement based on virtual impedance for dc microgrids with constant power loads. IEEE Trans Smart Grid 2015;6(6):2770–83. Nov.
[11] Kwasinski A, Onwuchekwa CN. Dynamic behavior and stabilization of dc microgrids with instantaneous constant-power loads. IEEE Trans Power Electron 2011;26(3):822–34. March.
[12] Feng X, Ye Z, Xing K, Lee FC, Borojevic D. Impedance specification and impedance improvement for dc distributed power system. In: 30th Annual IEEE Power Electronics Specialists Conference, vol. 2; July 1999. p. 889–94.
[13] Liu J, Zhang W, Rizzoni G. Robust stability analysis of dc microgrids with constant power loads. IEEE Trans Power Syst 2018;33(1):851–60. January.
[14] Su M, Liu Z, Sun Y, Han H, Hou X. Stability analysis and stabilization methods of dc microgrid with multiple parallel-connected DC-DC converters loaded by CPLs. IEEE Trans Smart Grid 2018;9(1):132–42. January.
[15] Herrera L, Zhang W, Wang J. Stability analysis and controller design of DC microgrids with constant power loads. IEEE Trans Smart Grid 2017;8(2):881–8. March.
[16] You J, Vilathgamuwa M, Ghasemi N. DC bus voltage stability improvement using disturbance observer feedforward control. Control Eng Practice 2018;75:118–25.
[17] Yang N, Nahid-Mobarakeh B, Gao F, Paire D, Miraoui A, Liu W. Modeling and stability analysis of multi-time scale dc microgrid. Electr Power Syst Res 2016;140:906–16.
[18] Rashidirad N, Hamzeh M, Sheshyekani K, Afjei E. A simplified equivalent model for the analysis of low-frequency stability of multi-bus DC microgrids. IEEE Trans Smart Grid 2018;9(6):6170–82. November.
[19] Chen X, Shi M, Sun H, Li Y, He H. Distributed cooperative control and stability analysis of multiple DC electric springs in a DC microgrid. IEEE Trans Industr Electron July 2018;65(7):5611–22.
[20] Yuan M, Fu Y, Mi Y, Li Z, Wang C. Hierarchical control of DC microgrid with dynamical load power sharing. Appl Energy 2019;239:1–11.
[21] Mojica-Nava E, Rey JM, Torres-Martinez J, Castilla M. Decentralized switched current control for DC microgrids. IEEE Trans Industr Electron 2019;66(2):1182–91. February.
[22] Kumar J, Agarwal A, Agarwal V. A review on overall control of DC microgrids. J Energy Storage 2019;21:113–38.
[23] Vu TV, Gonsoulin D, Perkins D, Papari B, Vahedi H, Edrington CS. Distributed control implementation for zonal MVDC ship power systems. In: Proceedings of IEEE Electric Ship Technologies Symposium (ESTS); Aug 2017. p. 539–43.
[24] Chen Y, Zhao S, Li Z, Wei X, Kang Y. Modeling and control of the isolated DC-DC modular multilevel converter for electric ship medium voltage direct current power system. IEEE J Emerg Sel Top Power Electron 2017;5(1):124–39. March.
[25] Haseltalab A, Botto MA, Negenborn RR. On-board voltage regulation for all-electric dc ships. IFAC-PapersOnLine 2018;51(29):341–7.
[26] Haseltalab A, Negenborn RR. Model predictive maneuvering control and energy management for all-electric autonomous ships. Appl Energy 2019;251:113308.
[27] Meng L, Shafiee Q, Trecate GF, Karimi H, Fulwani D, Lu X, et al. Review on control of dc microgrids and multiple microgrid clusters. IEEE J Emerg Sel Top Power Electron 2017;5(3):928–48. September.
[28] Rawlings JR, Mayne DQ. Model Predictive Control: Theory and Design. Nob Hill Publishing; 2009.

[29] te Braake HAB, Botto MA, van Can HJL, da Costa JS, Verbruggen HB. Linear predictive control based on approximate input-output feedback linearisation. IEE Proc Control Theory Appl July 1999;146(4):295–300.
[30] Kurtz MJ, Henson MA. Input-output linearizing control of constrained nonlinear processes. J Process Control 1997;7(1):3–17.
[31] Hou J, Song Z, Hofmann H, Sun J. Adaptive model predictive control for hybrid energy storage energy management in all-electric ship microgrids. Energy Convers Manage 2019;198:111929.
[32] van Biert L, Godjevac M, Visser K, Aravind PV. A review of fuel cell systems for maritime applications. J Power Sour 2016;327:345–64.
[33] Zahedi B, Norum L. Modeling and simulation of all-electric ships with low-voltage dc hybrid power systems. IEEE Trans Power Electron 2013;28(10):4525–37. October.
[34] Izadi-Zamanabadi R, Blanke M. A ship propulsion system as a benchmark for fault-tolerant control. Control Eng Practice 1999;7(2):227–39.
[35] Geertsma R, Negenborn R, Visser K, Loonstijn M, Hopman J. Pitch control for ships with diesel mechanical and hybrid propulsion: Modelling, validation and performance quantification. Appl Energy 2017;206:1609–31.
[36] Blanke M, Andersen J. On Dynamics of Large Two Stroke Diesel Engines: New Results from Identification. IFAC Proc Vol 1984;17(2):2015–20.
[37] Smogeli ON. Control of marine propellers [Ph.D. dissertation]. Norwegian University of Science and Technology (NTNU); 2006.
[38] Fitzgerald JAE, Kingsley Charles, Umans SD. Electric Machinery - Sixth Edition. McGraw-Hill; 2003.
[39] Krause PC, Wasynczuk O, Sudhoff SD, Pekarek S. Analysis of Electric Machinery and Drive Systems. 3rd ed. Wiley; 2013.
[40] Jatskevich J, Pekarek SD, Davoudi A. Parametric average-value model of synchronous machine-rectifier systems. IEEE Trans Energy Convers 2006;21(1):9–18. March.
[41] Plett GL. Extended Kalman filtering for battery management systems of LiPb-based HEV battery packs: Part 1. background. J Power Sources 2004;134(2):252–61.
[42] Syverud TH. Modeling and control of a dc-grid hybrid power system with battery and variable speed diesel generators [Master's thesis]. Norwegian University of Science and Technology; 2016.
[43] Henson MA, Seborg DE, editors. Nonlinear Process Control. Upper Saddle River, NJ, USA: Prentice-Hall, Inc.; 1997.
[44] Geertsma R. Autonomous control for adaptive ships with hybrid propulsion and power generation [Ph.D. dissertation]; 2019.